Received: 6 September 2023 | Accepted: 11 September 2023

DOI: 10.1002/nano.202300130

RESEARCH ARTICLE

Nano Select WILEY

Remediation of charged organic pollutants—binding motifs for highly efficient water cleaning with nanoparticles

Andreas Eigen[1] | **Victoria Schmidt**[1] | **Marco Sarcletti**[1] | **Selina Freygang**[1] | **Andreas Hartmann-Bausewein**[1] | **Vanessa Schneider**[1] | **Anna Zehetmeier**[1] | **Vincent Mauritz**[2] | **Lukas Müller**[1] | **Henrik Gaß**[1] | **Linda Rockmann**[1] | **Ryan W. Crisp**[2] | **Marcus Halik**[1]

[1]Organic Materials & Devices, Institute of Polymer Materials, Department of Materials Science, Friedrich-Alexander-Universität Erlangen-Nürnberg, Erlangen, Germany

[2]Chemistry of Thin Film Materials, Department of Chemistry and Pharmacy Friedrich-Alexander-Universität Erlangen-Nürnberg Egerlandstrasse 1, Erlangen, Germany

Correspondence
Marcus Halik, Organic Materials & Devices, Institute of Polymer Materials, Department of Materials Science, Friedrich-Alexander-Universität Erlangen-Nürnberg, INZF, Cauerstraße 3, 91058 Erlangen, Germany.
Email: marcus.halik@fau.de

Funding information
Deutsche Bundesstiftung Umwelt; Deutsche Forschungsgemeinschaft, Grant/Award Number: 2952/10-1

Abstract

Many charged organic molecules behave as persistent and hazardous pollutants with harmful effects on human health and ecosystems. They are widely distributed related to their charged molecular structure that provides water solubility. In order to track the fate and behavior of such pollutants, charged dyes with specific absorption in the visible spectra serve as convenient model compounds. We provide a platform of smart adsorbers that efficiently remediate positively and negatively charged dyes (crystal violet and Amaranth) from water. Metal oxide nanoparticles serve as a core with an intrinsically large surface area. The surface potential was tuned towards positive or negative by decorating the cores with self-assembled monolayers of dedicated long-chained phosphonic acid derivatives. Selective remediation of the dyes was obtained with corresponding oppositely charged core-shell nanoparticles. Mixed dye solution can be cleaned by a cascade approach or by applying both particle systems simultaneously. The removal efficiency was determined as a function of particle concentration via UV-spectroscopy. The results of remediation experiments at different pH values and using superparamagnetic iron oxide nanoparticle cores lead to a simple process with recycling capability.

KEYWORDS
phosphonic acids, selectivity, self-assembled monolayer, surface chemistry, water remediation

1 | INTRODUCTION

In our anthropogenically driven world, drinking water supplies are dwindling everywhere, and water pollution with organic substances that are persistent and hazardous is steadily increasing.[1–4] In particular, those contaminants with polar or charged moieties exhibit improved solubility in water and tend to dilute so that they widely distribute and occur in trace concentrations.[5] Some organic dyes also count as problematic contaminants and are used in large quantities in the textile and food industry.[6–9]

In contrast to most organic molecules composed of a sp3-carbon skeleton, such dyes exhibit conjugated π-systems.[10,11] That leads to pronounced light absorption of different dyes at a dedicated wavelength as a function of their structure, and they can be easily detected and tracked by simple optical spectroscopic methods. Water-soluble dyes are thus perfect model representatives for other charged organic pollutants. Charged organic dyes can be classified by their Coulomb charge.[7,12] Cationic dyes tend to interact with the negative surface charge of cell membranes, enabling cell penetration.[13,14]

On the other hand, anionic molecules are known for their reactivity due to hydrolysis in an aqueous environment and their harmful effects on the human body as they often contain sulfonic acid groups.[12] Crystal violet ($\mathbf{CV}^+$), a common cationic triphenylmethane dye, and amaranth ($\mathbf{AM}^-$), an anionic azo dye, were selected for our study. $\mathbf{CV}^+$ is known next to other hazardous impacts for its mutagenic and potent carcinogenic effects.[13,14] $\mathbf{AM}^-$ is known for causing different severe diseases, including congenital disabilities and tumors.[15,16] Besides their environmental impact, both dyes represent either cationic or anionic organic pollutants that need to be removed from water with a simple, inexpensive, and scalable method.

Many different processes have been developed to purify water from organic pollutants, such as chemical methods like photocatalytic[17,18] or electrochemical[2,19–21] oxidation, ozonation,[22] and flocculation,[23–25] physical methods like filtration[26] and adsorption[8,9,27–33] or biological processes like bioremediation[34–38] utilizing bacteria and fungi, or enzymatic decomposition.[39] The adsorption of pollutants on surfaces is one of the most promising methods.[9] Thereby, inexpensive broadband materials are typically used as stationary phase filters—for example, active carbon[40] or minerals.[41,42] However, those approaches are limited in loading capacity and selectivity. Mobile sorbent materials that flow within the water phase attract pollutants efficiently and can finally be removed, representing a novel class of systems.[43] Metal oxide nanoparticles (e.g., alumina, iron oxide, titanium oxide, or zinc oxide) are accessible in sizeable quantities and provide a large intrinsic surface for adsorption. Additionally, nanoparticle surfaces can be functionalized to introduce different surface properties.[44] Several studies have treated nanoparticles (NPs) with amphiphiles such as sodium dodecyl sulfate (SDS) or cetrimonium bromide (CTAB) to improve their adsorption behavior.[45] However, these surface additives may cause secondary pollution of water bodies as they are only physisorbed and, therefore, reversibly attached to the surface. Other methods use complex core-shell systems, for example, consisting of an iron oxide core with a silica shell to anchor ligands to the surface.[46] In order to create a large surface area with dedicated, attractive interaction motifs, long-chained phosphonic acid (PA) derivatives have been established.[43,47–55] PAs tend to form self-assembled monolayers (SAMs), providing long-term stable binding on metal oxide surfaces.[56,57] Core-shell NPs with PA-SAMs have been demonstrated as efficient sorbent materials to remove hydrophobic alkanes, crude oil, aromatic compounds, and even nano- and microplastics.[43,47,49]

In this work, we investigate the selectivity in removing charged organic molecules. We have functionalized aluminum oxide nanoparticles (**AlOx**-NPs) with two different phosphonic acid derivatives (Figure 1A) to realize core-shell NPs that exhibit either positive (red) or negative (blue) surface charge. Those systems are designed to behave complementarily to the charges of the proposed dyes, $\mathbf{AM}^-$ and $\mathbf{CV}^+$ (Figure 1B). N-octadecyl phosphonic acid ($\mathbf{PAC_{18}}$) and (12-dodecyl phosphonic acid)-N-N-dimethyl-N-octadecyl ammonium chloride ($\mathbf{PAC_{12}NC_{18}}$) were used as SAM-building molecules. In addition to the central electrostatic interaction motif of charge and surface charge, the SAM functionalization introduces secondary motifs as Van der Waals (vdW) forces for all intermolecular and hydrophobic interactions of long chains of the SAM molecules and the conjugated core of the dyes. The removal of dyes from water has been demonstrated individually for each dye and simultaneously in cascade experiments (Figure 1C). Investigating the pH dependency of the adsorption and the desorption of contaminants leads to a potential green process of particle recycling using acids and bases. Finally, by utilizing maghemite NPs ($\mathbf{Fe_2O_3}$-NPs) instead of **AlOx**-NPs as core material, the collection process can be performed by applying an external magnetic field, which offers large-scale applications. All these findings combined make it a universal tool for water remediation of charged organic pollutants.

2 | RESULTS AND DISCUSSION

AlOx NPs, as well as $\mathbf{Fe_2O_3}$-NPs, were characterized by BET, transmission electron spectroscopy (TEM), X-ray diffraction (XRD), and dynamic light scattering (DLS). TEM measurements on **AlOx** NPs confirm the manufacturer's specification of particle sizes below 50 nm (Figure S4). Similar measurements on $\mathbf{Fe_2O_3}$-NPs have already been published elsewhere.[43] XRD measurements are shown in Figure S5. These measurements confirm the nanocrystalline structure, as Scherrer analysis gave crystallite sizes of 6.6 nm for **AlOx** NPs and 9.1 nm for $\mathbf{Fe_2O_3}$-NPs. Additionally, the measurements confirmed the crystal structures of the two materials to be the monoclinic γ-Al_2O_3 and the cubic maghemite structure of $\mathbf{Fe_2O_3}$

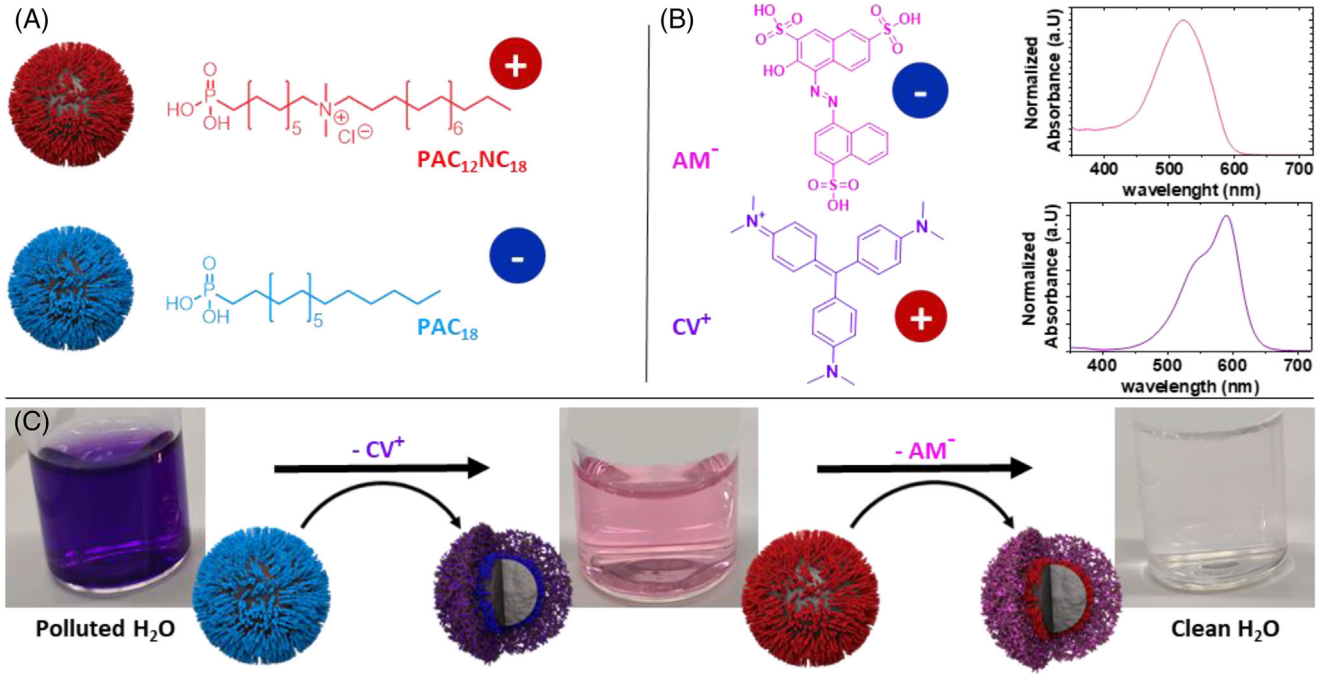

FIGURE 1 Schematic outline for removal of charged molecules with (A) functionalized **AlOx** nanoparticles (schematic representation with chemical formulas of $\mathbf{PAC_{18}}$ and $\mathbf{PAC_{12}NC_{18}}$). B, Chemical formulas and UV-Vis spectra of the used contaminant molecules Amaranth ($\mathbf{AM^-}$) and crystal violet ($\mathbf{CV^+}$). C, Photographs of the water cleaning principle together with a schematic explanation, where a mixture of $\mathbf{CV^+}$ and $\mathbf{AM^-}$ is first treated with $\mathbf{PAC_{18}}$ functionalized NPs ($\mathbf{PAC_{18}}$-NPs) to remove the positively charged $\mathbf{CV^+}$ and subsequently treated with $\mathbf{PAC_{18}}$ functionalized NPs ($\mathbf{PAC_{12}NC_{18}}$-NPs) to remove the negatively charged $\mathbf{AM^-}$.

of the two materials. BET measurements gave specific surface areas of 123.6 m2 g^{-1} for **AlOx**-NPs and 111.8 m2 g^{-1} for $\mathbf{Fe_2O_3}$-NPs. DLS measurements in water showed average particle diameters for **AlOx**-NPs of 80 nm ± 26 nm, indicating agglomeration.

The particles have been functionalized with $\mathbf{PAC_{18}}$ and $\mathbf{PAC_{12}NC_{18}}$ according to the method described in SI. In order to quantify the shell formation, the particles were analyzed by thermogravimetry (TGA). The measurements showed an increased mass loss (15.5% and 7.2%, respectively) for both $\mathbf{PAC_{18}}$ and $\mathbf{PAC_{12}NC_{18}}$ functionalized nanoparticles ($\mathbf{PAC_{18}}$-NPs and $\mathbf{PAC_{12}NC_{18}}$ NPs) compared to pristine **AlOx**-NPs (Figure S1A). These losses correspond to a grafting density (GD) of 3.66 and 0.74 nm^{-2}. The lower GD for $\mathbf{PAC_{12}NC_{18}}$-NPs compared to neutral n-alkyl-chained $\mathbf{PAC_{18}}$ can be explained by repulsive Coulomb forces of the charged quaternary amine and the extended space demand related to the methyl-substitution. The GD of $\mathbf{PAC_{18}}$-NPs agrees with the literature for a fully covered surface.[43,49,56] Fourier-transform infrared spectroscopy (FTIR) was used to qualify the corresponding SAM features on the NP surfaces (Figure S2A). The spectra of both systems exhibit clear alkyl chain signals at 2850 cm^{-1} and 2930 cm^{-1}, together with signals for bound phosphonic acid at around 1000 cm^{-1}. XRD measurements (Figure S5) before and after functionalization showed no difference, indicating that the particles do not change in size or crystal structure during functionalization.

The NP dispersibility and surface charge were investigated by pH-dependent zeta potential measurements (Figure S3A). Both particle systems show zeta potentials between −40 and 40 mV but with different isoelectric points (IEP). $\mathbf{PAC_{18}}$-NPs showed an IEP at pH 6.9, whereas $\mathbf{PAC_{12}NC_{18}}$-NPs had an IEP at pH 9.4 due to the quaternary ammonium moiety (pristine **AlOx**-NPs showed an IEP at pH 9.0). At a neutral pH (pH7), the $\mathbf{PAC_{18}}$-NPs show a zeta potential of −2.0 ± 5.7 mV, making them almost neutral but slightly negatively charged, while $\mathbf{PAC_{12}NC_{18}}$-NPs show a positive zeta potential of +30.5 ± 11.6 mV.

Additionally, both SAMs inherit an alkylated chain pointing outwards, which makes them hydrophobic. Static contact angle measurements were conducted on flat atomic layer deposited (ALD) surfaces functionalized with the SAMs to confirm the hydrophobic character of surfaces functionalized with either of the two SAMs (Table S1). The experiment was conducted on a flat surface rather than spray-coated NPs to avoid inaccuracies due to different surface roughness. $\mathbf{PAC_{18}}$-surfaces showed hydrophobic behavior with a contact angle of 106.9° to water. The contact angle is reduced to 71.5° for $\mathbf{PAC_{12}NC_{18}}$ but still significantly increased compared to the pristine ALD wafer surface, which showed a contact angle of 28.3°. Thus,

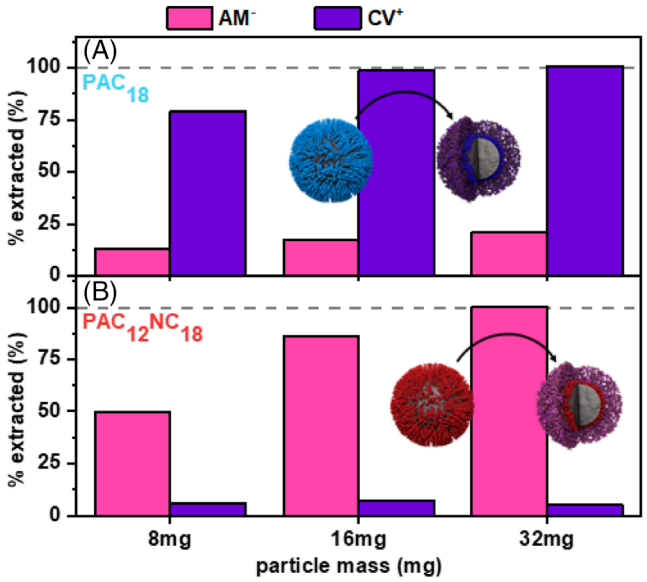

FIGURE 2 Influence of the particle mass on $\mathbf{AM}^-$ and $\mathbf{CV}^+$ removal efficiency with (A) $\mathbf{PAC_{18}}$**-NPs** and (B) $\mathbf{PAC_{12}NC_{18}}$**-NPs**.

the $\mathbf{PAC_{12}NC_{18}}$-NPs showed hydrophobic behavior even with the lower grafting density. The hydrophobicity and the zeta potential can be tuned in that range by mixing the two SAMs in different ratios (Figure S3). This concept of mixed SAMs can increase water dispersibility and maintain the hydrophobic character. Similar results were found for $\mathbf{Fe_2O_3}$-NPs with grafting densities of 0.73 and 2.39 nm^{-2} for $\mathbf{PAC_{12}NC_{18}}$-$\mathbf{Fe_2O_3}$ and $\mathbf{PAC_{18}}$-$\mathbf{Fe_2O_3}$, respectively (Figure S1B), and FTIR spectra of phosphonic acid and alkyl chain bands were obtained (Figure S2B). The IEPs were slightly lower than for **AlOx**-NPs, with pH 8.0 for $\mathbf{PAC_{12}NC_{18}}$-$\mathbf{Fe_2O_3}$ and pH 5.4 for $\mathbf{PAC_{18}}$-$\mathbf{Fe_2O_3}$ (Figure S3B).

2.1 | Investigation of the maximum loading capacity

To study the maximum loading capacity, water samples with a volume of 14 mL containing either 0.036 mM of $\mathbf{AM}^-$ or $\mathbf{CV}^+$ were treated with particle amounts of 8 mg, 16 mg, and 32 mg for each NP-system (Figure 2). The pH value was set to pH 7 to investigate the adsorption behavior under neutral conditions. 16 mg of $\mathbf{PAC_{18}}$-NPs was sufficient to remove $\mathbf{CV}^+$ completely (below the detection limit, which is 0.1 µM for $\mathbf{CV}^+$ and $\mathbf{AM}^-$ for our method), and 32 mg of $\mathbf{PAC_{12}NC_{18}}$-NPs were needed to achieve the same result for $\mathbf{AM}^-$. Both systems showed high selectivity towards the oppositely charged contaminant. With 8 mg of $\mathbf{PAC_{18}}$-NPs, extraction rates for $\mathbf{AM}^-$ of 12.9% and 78.8% for $\mathbf{CV}^+$ were achieved (Figure 2A). Contrarily, $\mathbf{PAC_{12}NC_{18}}$-NPs extract $\mathbf{AM}^-$ with a rate of 49.5% and $\mathbf{CV}^+$ with a rate of 5.7% (Figure 2B). $\mathbf{AM}^-$ has three negative charges, while $\mathbf{CV}^+$ has a positive charge (Figure 1). The negatively charged $\mathbf{PAC_{18}}$-NPs attracted the oppositely charged contaminant $\mathbf{CV}^+$ but not $\mathbf{AM}^-$ electrostatically.

Nonetheless, other attractive binding motifs like vdW or hydrophobic interactions also play a crucial role. These interactions can explain the small fraction of $\mathbf{AM}^-$ extracted by $\mathbf{PAC_{18}}$-NPs. Weaker hydrophobic interactions could explain the lower extraction rates of $\mathbf{PAC_{12}NC_{18}}$ compared to $\mathbf{PAC_{18}}$, as the GD for $\mathbf{PAC_{12}NC_{18}}$ was significantly lower, and the surface energy increased (Figure S1A and Table S1). Still, both systems could outperform the pristine nanoparticles, which captured $\mathbf{AM}^-$ and $\mathbf{CV}^+$ with 42.1% and 20.8% extraction rates, respectively (Figure S6). As the remaining water treated with 8 mg of nanoparticles still contained significant amounts of dye molecules, it can be assumed that the particles were fully loaded with their maximum capacity. The packing density of the contaminants on the surfaces of the particles was estimated to get a deeper insight into the adsorption mechanisms. With a surface area of 123 m2 g^{-1} (according to BET measurements) of pristine **AlOx**-NPs, the extraction rates of $\mathbf{AM}^-$ with $\mathbf{PAC_{12}NC_{18}}$-NPs are 0.15 nm^{-2} (18.9 mg g^{-1}), and $\mathbf{CV}^+$ with $\mathbf{PAC_{18}}$-NPs are 0.23 nm^{-2} (20.1 mg g^{-1}). The calculation indicates that at maximum loading, a monolayer of dyes is attracted around the particle until the point is reached where the particle's charge is balanced and repulsion occurs between the dye molecules. The fact that the concentrations of realistic water pollution in wastewater treatment plants are 1000 times smaller (in the order of ng L^{-1}) indicates that 1.6 g of these particles is sufficient to clean 1 m^3 of water, making it a highly efficient water remediation method.

Nevertheless, a scalable extraction method needs to be selected for cleaning the amounts of water a treatment plant faces. A promising approach is using superparamagnetic iron oxide nanoparticles ($\mathbf{Fe_2O_3}$-NPs) instead of **AlOx**-NPs since these can be easily removed by applying an external magnetic field.[43,47,49,58] The proof of concept for magnetic remediation of charged dyes is shown in Figure S7. The extraction rates for $\mathbf{PAC_{18}}$-$\mathbf{Fe_2O_3}$-NPs of 93.2% (for $\mathbf{CV}^+$) and 6.1% (for $\mathbf{AM}^-$) and $\mathbf{PAC_{12}NC_{18}}$-$\mathbf{Fe_2O_3}$-NPs of 31.1% (for $\mathbf{CV}^+$) and 22.6% (for $\mathbf{AM}^-$) are similar as for **AlOx**-NPs and corresponding centrifugation as a separation method.

2.2 | Cascade extraction

To further investigate the selective binding in competition, $\mathbf{PAC_{18}}$-NPs and $\mathbf{PAC_{12}NC_{18}}$-NPs were added consecutively to a dye mixture consisting of an equimolar solution

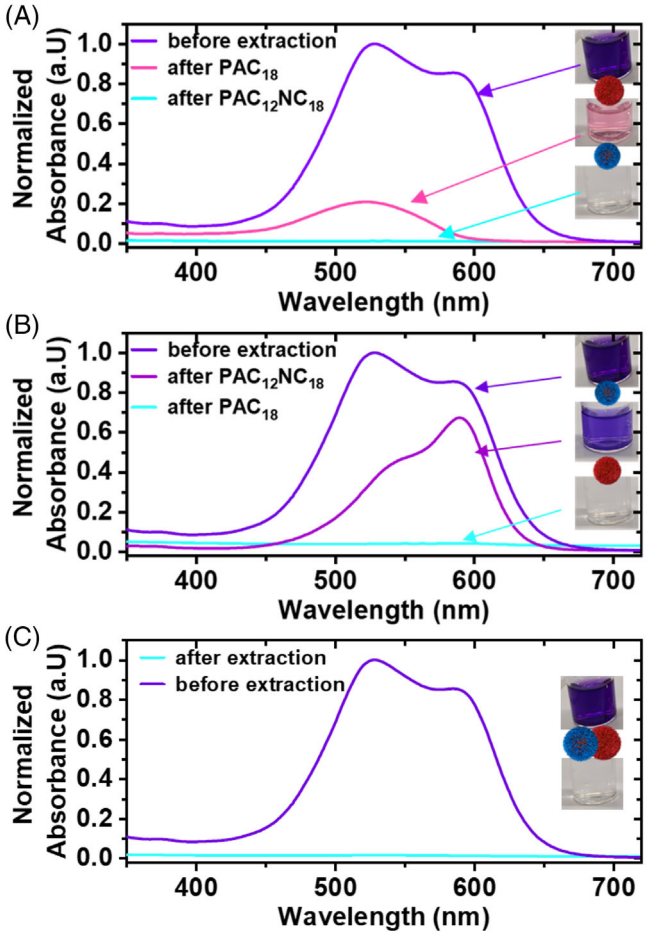

FIGURE 3 UV/Vis spectra of water samples contaminated with a mixture of CV^+ and AM^- and treated by (A) **PAC_{18}-NPs** in the first step and **$PAC_{12}NC_{18}$-NPs** in the second step, (B) **$PAC_{12}NC_{18}$-NPs** in the first step and **PAC_{18}-NPs** in a second step, and (C) both particle systems simultaneously. The photographs show the initial dye mixture and the remaining supernatants after each extraction step.

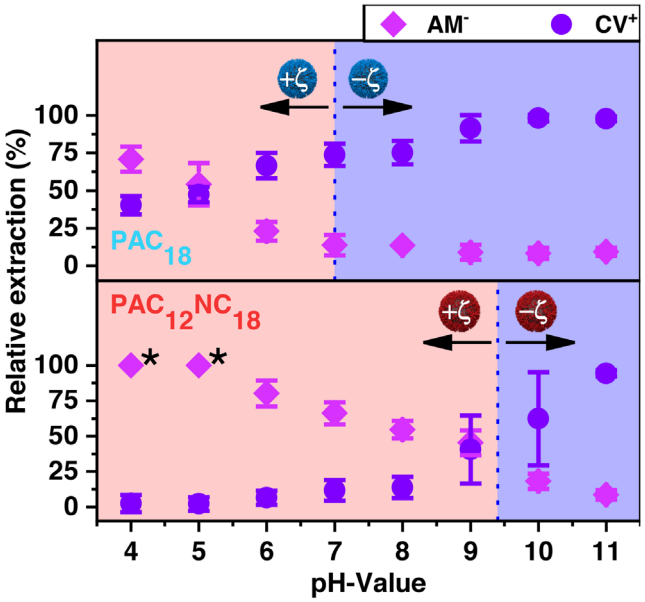

FIGURE 4 Effect of the pH value on contaminant adsorption onto **$PAC_{12}NC_{18}$**-NPs and **PAC_{18}**-NPs. The dotted vertical line indicates the IEP of the nanoparticles. The red and blue areas mark the region where the particles show a positive (red) or negative (blue) zeta potential. The error bars in the figure show the standard deviation obtained from at least three replicates. The measurements marked with * were set to 100%, indicating that the measurement did not detect the contaminant.

of AM^- and CV^+ with a concentration of 0.05 mM (Figure 3). After treatment of the solution with **PAC_{18}**-NPs (Figure 3A), the initial color changes, and a clear AM^- signal (see also Figure 1) was left in the supernatant. The negatively charged **PAC_{18}**-NPs favor the adsorption of CV^+. By subsequently adding **$PAC_{12}NC_{18}$**-NPs to that supernatant, the remaining AM^- signal was removed, leading to clear, non-colored, clean water. On the opposite, when the positively charged **$PAC_{12}NC_{18}$**-NPs were added first to the dye mixture (Figure 3B), a clear signal of CV^+ remained due to the removal of the negatively charged AM^-, which was subsequently removed in the second step by adding **PAC_{18}**-NPs.

In addition to these cascade or cross experiments, particle systems can be added simultaneously to the mixed dye solution. That immediately leads to clean, non-colored water without a detectable signal in the UV/VIS spectra (Figure 3C). This experiment proves the possibility of removing oppositely charged contaminants in an easy one-step process.

2.3 | Influence of the pH value

As the pH value strongly impacts the zeta potential of functionalized particles and thereby might impact technical/practical remediation processes, we have determined the zeta potential of our systems for pH values ranging from 4 to 11 (Figure S3). Additionally, we have performed corresponding remediation experiments at different pH values (Figure 4). The extraction rate for AM^- decreases from 70.9% to 9.2% for **PAC_{18}**-NPs and 100% (not detectable anymore with the used method) to 8.4% for **$PAC_{12}NC_{18}$**-NPs with increasing pH value while the extraction rate for CV^+ increases (from 40.3% to 98.9% for **PAC_{18}**-NPs and from 2.1% to 95.7% for **$PAC_{12}NC_{18}$**-NPs). As the particles become more and more negatively charged with increasing pH value, this could be explained by the electrostatic interactions attracting or repulsing the dye contaminants. With that, the pH-dependency to the selective binding towards one of the dye molecules discussed before can be altered

and even reversed. The dependence on the pH value thus opens the door for a simple and eco-friendly recycling process by washing the loaded particles at a suitable pH value. Exemplarily washing was tested for **PAC$_{18}$**-NPs, primarily loaded with **AM**$^-$ at pH4 and **CV**$^+$ at pH10 (Figure S8). The first results support that **AM**$^-$ was reversibly desorbed at high pH values, and up to 99.5% could be recovered at pH 11. **CV**$^+$, on the other hand, showed the strongest desorption at pH 3 with a desorption efficiency of 31.8%.

However, high extraction rates were achieved for both dyes in the medium pH range (pH 6 to 8) even though the particles have the same charge as the contaminant. We assume that the hydrophobic segregation, related to the π-core structure of the dyes and expressed by solubility in water (10 mg mL^{-1} for **CV**$^+$ and 50 mg mL^{-1} for **AM**$^-$), becomes a significant driving force to the hydrophobic NP-surface.

3 | CONCLUSION

We have generated oppositely surface-charged nanoparticles by self-assembling dedicated chained phosphonic acid ligands. These modified NPs exhibit excellent adsorption properties for either anionic or cationic dye molecules with high selectivity to the oppositely charged molecules. Mixed contaminated water samples containing the two charged dyes can be selectively cleaned stepwise in any order or simultaneously with excellent efficiency. The pH dependency of dye-NP-surface attraction can be used to reverse the selectivity, thereby offering a tool to recycle the particles. The concept was successfully applied to superparamagnetic iron oxide nanoparticles. Selectivity and recyclability, combined with simple magnetic remediation, provide the potential for a green and eco-friendly process. Altogether, we firmly believe that this simple and universal tool could be used to clean water from various charged organic contaminants.

ACKNOWLEDGMENTS

The authors are grateful for financial support by the Graduate School Molecular Science (GSMS), the Deutsche Forschungsgemeinschaft (DFG) project HA 2952/10-1, and Deutsche Bundesstifutung Umwelt (DBU, German Federal Environmental Foundation). L.M. acknowledges scholarship funding by the Deutsche Bundesstiftung Umwelt (DBU 20021/713, German Federal Environmental Foundation). R.W.C. and V.M. acknowledge financial support of the Engineering of Advanced Materials (EAM) Competence Center at FAU. The manuscript was written through the contributions of all authors. All authors have given approval for the final version of the manuscript.

Open access funding enabled and organized by Projekt DEAL.

CONFLICT OF INTEREST STATEMENT

The authors declare no conflicts of interest.

DATA AVAILABILITY STATEMENT

The data that support the findings of this study are available from the corresponding author upon reasonable request.

REFERENCES

1. Z. Wang, R. Altenburger, T. Backhaus, A. Covaci, M. L. Diamond, J. O. Grimalt, R. Lohmann, A. Schäffer, M. Scheringer, H. Selin, A. Soehl, N. Suzuki, *Science (80)*. **2021**, *371*(6531), 774. https://doi.org/10.1126/science.abe9090
2. M. G. Evich, M. J. B. Davis, J. P. McCord, B. Acrey, J. A. Awkerman, D. R. U. Knappe, A. B. Lindstrom, T. F. Speth, C. Tebes-Stevens, M. J. Strynar, Z. Wang, E. J. Weber, W. M. Henderson, J. W. Washington, *Science (80-)* **2022**, *375*(6580). https://doi.org/10.1126/science.abg9065
3. S. C. Doney, *Science (80-)* **2010**, *328*(5985), 1512. https://doi.org/10.1126/science.1185198
4. J. E. Elliott, K. H. Elliott, *Science (80-)* **2013**, *340*(6132), 556. https://doi.org/10.1126/science.1235197
5. T. Reemtsma, U. Berger, H. P. H. Arp, H. Gallard, T. P. Knepper, M. Neumann, J. B. Quintana, P. D. Voogt, *Environ. Sci. Technol.* **2016**, *50*(19), 10308–10315. https://doi.org/10.1021/acs.est.6b03338
6. M. M. Hassan, C. M. Carr, *Chemosphere* **2021**, *265*, 129087. https://doi.org/10.1016/j.chemosphere.2020.129087
7. S. K. Panda, I. Aggarwal, H. Kumar, L. Prasad, A. Kumar, A. Sharma, D.-V. N. Vo, D. Van Thuan, V. Mishra, *Environ. Chem. Lett.* **2021**, *19* (3), 2487. https://doi.org/10.1007/s10311-020-01173-9
8. M. El Khomri, N. El Messaoudi, A. Dbik, S. Bentahar, A. Lacherai, Z. Goodarzvand Chegini, M. Iqbal, *Biointerface Res. Appl. Chem.* **2021**, *12* (2), 2022. https://doi.org/10.33263/BRIAC122.20222040
9. M. Oppmann, M. Wozar, J. Reichstein, K. Mandel, *ChemNanoMat* **2018**, *5*(2), cnma.201800490. https://doi.org/10.1002/cnma.201800490
10. A. I. Kiprianov, *Russ. Chem. Rev.* **1971**, *40*(7), 594. https://doi.org/10.1070/RC1971v040n07ABEH001942
11. M. Ejder-Korucu, A. Gürses, Ç. Doğar, S. K. Sharma, M. Açıkyıldız, *Green chemistry for dyes removal from wastewater*, Wiley, **2015**, pp 1. https://doi.org/10.1002/9781118721001.ch1
12. M. A. M. Salleh, D. K. Mahmoud, W. A. W. A. Karim, A. Idris, *Desalination* **2011**, *280*(1–3), 1. https://doi.org/10.1016/j.desal.2011.07.019
13. K. P. Singh, S. Gupta, A. K. Singh, S. Sinha, *J. Hazard. Mater.* **2011**, *186*(2–3), 1462. https://doi.org/10.1016/j.jhazmat.2010.12.032
14. S. Li, *Bioresour. Technol.* **2010**, *101*(7), 2197. https://doi.org/10.1016/j.biortech.2009.11.044
15. A.-N. M. Salem, M. A. Ahmed, M. F. El-Shahat, *J. Mol. Liq.* **2016**, *219*, 780. https://doi.org/10.1016/j.molliq.2016.03.084

16. P. Mpountoukas, A. Pantazaki, E. Kostareli, P. Christodoulou, D. Kareli, S. Poliliou, C. Mourelatos, V. Lambropoulou, T. Lialiaris, *Food Chem. Toxicol.* **2010**, *48*(10), 2934. https://doi.org/10.1016/j.fct.2010.07.030
17. N. Qutub, P. Singh, S. Sabir, S. Sagadevan, W.-C. Oh, *Sci. Rep.* **2022**, *12* (1), 5759. https://doi.org/10.1038/s41598-022-09479-0
18. K. O. Sodeinde, S. O. Olusanya, O. S. Lawal, M. Sriariyanun, A. A. Adediran, *Sci. Rep.* **2022**, *12*(1), 17054. https://doi.org/10.1038/s41598-022-21266-5
19. T. Droguett, J. Mora-Gómez, M. García-Gabaldón, E. Ortega, S. Mestre, G. Cifuentes, V. Pérez-Herranz, *Sci. Rep.* **2020**, *10*(1), 4482. https://doi.org/10.1038/s41598-020-61501-5
20. D. H. S. Santos, J. L. S. Duarte, M. G. R. Tavares, M. G. Tavares, L. C. Friedrich, L. Meili, W. R. O. Pimentel, J. Tonholo, C. L. P. S. Zanta, *Chem. Eng. Process.—Process Intensif.* **2020**, *153*(February), 107940. https://doi.org/10.1016/j.cep.2020.107940
21. S. Garcia-Segura, A. B. Nienhauser, A. S. Fajardo, R. Bansal, C. L. Conrad, J. D. Fortner, M. Marcos-Hernández, T. Rogers, D. Villagran, M. S. Wong, P. Westerhoff, *Curr. Opin. Electrochem.* **2020**, *22*(March), 9. https://doi.org/10.1016/j.coelec.2020.03.001
22. M. Mehrjouei, S. Müller, D. Möller, *Chem. Eng. J.* **2015**, *263*, 209. https://doi.org/10.1016/j.cej.2014.10.112
23. J. El-Gaayda, F. E. Titchou, R. Oukhrib, P.-S. Yap, T. Liu, M. Hamdani, R. Ait Akbour, *J. Environ. Chem. Eng.* **2021**, *9*(5), 106060. https://doi.org/10.1016/j.jece.2021.106060
24. W. O. Leshniowsky, P. R. Dugan, R. M. Pfister, J. I. Frea, C. I. Randles, *Science (80-)* **1970**, *169*(3949), 993–995. https://doi.org/10.1126/science.169.3949.993
25. M. Lapointe, J. M. Farner, L. M. Hernandez, N. Tufenkji, *Environ. Sci. Technol.* **2020**, *54*(14), 8719. https://doi.org/10.1021/acs.est.0c00712
26. H. B. Park, J. Kamcev, L. M. Robeson, M. Elimelech, B. D. Freeman, *Science (80-)* **2017**, *356*(6343), 1138. https://doi.org/10.1126/science.aab0530
27. C. Osagie, A. Othmani, S. Ghosh, A. Malloum, Z. Kashitarash Esfahani, S. Ahmadi, *J. Mater. Res. Technol* **2021**, *14*, 2195. https://doi.org/10.1016/j.jmrt.2021.07.085
28. C. Namasivayam, R. Jeyakumar, R. T. Yamuna, *Waste Manag* **1994**, *14*(7), 643. https://doi.org/10.1016/0956-053X(94)90036-1
29. E. Loffredo, *Materials (Basel)* **2022**, *15*(5), 1894. https://doi.org/10.3390/ma15051894
30. M. T. Yagub, T. K. Sen, S. Afroze, H. M. Ang, *Adv. Colloid Interface Sci.* **2014**, *209*, 172. https://doi.org/10.1016/j.cis.2014.04.002
31. M. B. Wazir, M. Daud, F. Ali, M. A. Al-Harthi, *J. Mol. Liq.* **2020**, *315*, 113775. https://doi.org/10.1016/j.molliq.2020.113775
32. W. Li, C. Wu, Z. Xiong, C. Liang, Z. Li, B. Liu, Q. Cao, J. Wang, J. Tang, D. Li, *Sci. Adv.* **2022**, *8*(45), 1. https://doi.org/10.1126/sciadv.ade1731
33. A. A. Al-Gheethi, Q. M. Azhar, P. S. Kumar, A. A. Yusuf, A. K. Al-Buriahi, Radin Mohamed, M. S. R, M. M. Al-shaibani, *Chemosphere* **2022**, *287*(P2), 132080. https://doi.org/10.1016/j.chemosphere.2021.132080
34. L. R. S. Pinheiro, D. G. Gradíssimo, L. P. Xavier, A. V. Santos, *Sustainability* **2022**, *14*(3), 1510. https://doi.org/10.3390/su14031510
35. Y. Yang, J. Yang, L. Jiang, *Science (80-)* **2016**, *353*(6301), 75. https://doi.org/10.1126/science.aaf8305
36. J. Li, X. Li, Y. Da, J. Yu, B. Long, P. Zhang, C. Bakker, B. A. McCarl, J. S. Yuan, S. Y. Dai, *Nat. Commun.* **2022**, *13*(1), 4368. https://doi.org/10.1038/s41467-022-31881-5.
37. N. Ojha, R. Karn, S. Abbas, S. Bhugra, *IOP Conf. Ser. Earth Environ. Sci.* **2021**, *796*(1), 012012. https://doi.org/10.1088/1755-1315/796/1/012012
38. I. M. Head, D. M. Jones, W. F. M. Röling, *Nat. Rev. Microbiol.* **2006**, *4*(3), 173. https://doi.org/10.1038/nrmicro1348
39. M. Urso, M. Ussia, M. Pumera, *Nat. Rev. Bioeng.* **2023**, *1*(4), 236. https://doi.org/10.1038/s44222-023-00025-9
40. A. L. Duchesne, J. K. Brown, D. J. Patch, D. Major, K. P. Weber, J. I. Gerhard, *Environ. Sci. Technol.* **2020**, *54*(19), 12631. https://doi.org/10.1021/acs.est.0c03058
41. M. R. Abukhadra, A. S. Mohamed, *Silicon* **2019**, *11*(3), 1635. https://doi.org/10.1007/s12633-018-9980-3
42. B. O. Otunola, O. O. Ololade, *Environ. Technol. Innov.* **2020**, *18*, 100692. https://doi.org/10.1016/j.eti.2020.100692
43. M. Sarcletti, H. Park, J. Wirth, S. Englisch, A. Eigen, D. Drobek, D. Vivod, B. Friedrich, R. Tietze, C. Alexiou, D. Zahn, B. Apeleo Zubiri, E. Spiecker, M. Halik, *Mater. Today* **2021**, *48*(xx), 38. https://doi.org/10.1016/j.mattod.2021.02.020
44. A. Ulman, *Chem. Rev.* **1996**, *96*(4), 1533. https://doi.org/10.1021/cr9502357
45. F. Keyhanian, S. Shariati, M. Faraji, M. Hesabi, *Arab. J. Chem.* **2016**, *9*, S348. https://doi.org/10.1016/j.arabjc.2011.04.012
46. X. Zhang, H. Niu, Y. Pan, Y. Shi, Y. Cai, *J. Colloid Interface Sci.* **2011**, *362*(1), 107. https://doi.org/10.1016/j.jcis.2011.06.032
47. P. Groppe, S. Wintzheimer, A. Eigen, H. Gaß, M. Halik, K. Mandel, *Environ. Sci. Nano* **2022**, *9*(7), 2427. https://doi.org/10.1039/D2EN00131D
48. H. Park, J.-H. Kim, D. Vivod, S. Kim, A. Mirzaei, D. Zahn, C. Park, S. S. Kim, M. Halik, *Nano Today* **2021**, *40*, 101265. https://doi.org/10.1016/j.nantod.2021.101265
49. M. Sarcletti, D. Vivod, T. Luchs, T. Rejek, L. Portilla, L. Müller, H. Dietrich, A. Hirsch, D. Zahn, M. Halik, *Adv. Funct. Mater.* **2019**, *29*(15), 1805742. https://doi.org/10.1002/adfm.201805742
50. H. Park, J.-H. Kim, W.-S. Shin, A. Mirzaei, Y.-J. Kim, S. S. Kim, M. Halik, C. Park, *Sensors Actuators B Chem* **2022**, *372*, 132657. https://doi.org/10.1016/j.snb.2022.132657
51. S. Wenderoth, A. Eigen, S. Wintzheimer, J. Prieschl, A. Hirsch, M. Halik, K. Mandel, *Small* **2022**, *18*(15), 2107513. https://doi.org/10.1002/smll.202107513
52. C. Henkel, J. E. Wittmann, J. Träg, J. Will, L. M. S. Stiegler, P. Strohriegl, A. Hirsch, T. Unruh, D. Zahn, M. Halik, D. M. Guldi, *Small* **2020**, *16*(2), 1903729. https://doi.org/10.1002/smll.201903729
53. J. E. Wittmann, L. M. S. Stiegler, C. Henkel, J. Träg, K. Götz, T. Unruh, D. Zahn, A. Hirsch, D. Guldi, M. Halik, *Adv. Mater. Interfaces* **2019**, *6*(4), 1801930. https://doi.org/10.1002/admi.201801930
54. L. Portilla, M. Halik, *ACS Appl. Mater. Interfaces* **2014**, *6*(8), 5977. https://doi.org/10.1021/am501155r
55. A. Eigen, L. M. S. Stiegler, S. Gradl, V. Schneider, V. Wedler, H. Gaß, L. Müller, M. Sarcletti, M. R. Heinrich, A. Hirsch, M. Halik, *Adv. Mater. Interfaces* **2022**, *9*(32), 2201471. https://doi.org/10.1002/admi.202201471
56. L. Zeininger, L. Portilla, M. Halik, A. Hirsch, *Chem.—A Eur. J.* **2016**, *22*(38), 13506. https://doi.org/10.1002/chem.201601920

57. T. Bauer, T. Schmaltz, T. Lenz, M. Halik, B. Meyer, T. Clark, *ACS Appl. Mater. Interfaces* **2013**, *5*(13), 6073. https://doi.org/10.1021/am4008374
58. H. Park, A. May, L. Portilla, H. Dietrich, F. Münch, T. Rejek, M. Sarcletti, L. Banspach, D. Zahn, M. Halik, *Nat. Sustain.* **2019**, *3*(2), 129. https://doi.org/10.1038/s41893-019-0452-6

SUPPORTING INFORMATION

Additional supporting information can be found online in the Supporting Information section at the end of this article.

How to cite this article: A. Eigen, V. Schmidt, M. Sarcletti, S. Freygang, A. Hartmann-Bausewein, V. Schneider, A. Zehetmeier, V. Mauritz, L. Müller, H. Gaß, L. Rockmann, R. W. Crisp, M. Halik, *Nano Select* **2024**, *5*, 2300130. https://doi.org/10.1002/nano.202300130